Applied Catalysis B: Environmental 170-171 (2015) 273–282

Contents lists available at ScienceDirect

Applied Catalysis B: Environmental

journal homepage: www.elsevier.com/locate/apcatb

Polypropylene nonwoven filter with nanosized ZnO rods: Promising hybrid photocatalyst for water purification

Juan C. Colmenares[a,*], Ewelina Kuna[a], Szymon Jakubiak[b], Jakub Michalski[b], Krzysztof Kurzydłowski[b]

[a] Institute of Physical Chemistry PAS, Kasprzaka 44/52, 01-224 Warsaw, Poland
[b] Faculty of Materials Science and Engineering, Warsaw University of Technology, Woloska Str. 141, 02-507 Warsaw, Poland

ARTICLE INFO

Article history:
Received 27 November 2014
Received in revised form 20 January 2015
Accepted 23 January 2015
Available online 7 February 2015

Keywords:
1D Zinc oxide nanorods
Polypropylene nonwoven
Photocatalytic filter
Water purification
Phenol degradation

ABSTRACT

Modern composite filter materials were obtained via modification of commercially available polypropylene (PP) nonwovens with particles of nanorods zinc oxide (ZnO/PP) with high aspect ratio. This modification was conducted as a three-step process consisting of a plasma treatment of the polymer nonwovens (increasing their wettability), deposition of ZnO nuclei on fibers surface and low temperature hydrothermal growth of ZnO rods. A remarkable photocatalytic initial specific activity for ZnO/PP was observed (3-fold higher than commercial ZnO) and high stability in aqueous phase phenol mineralization.

1. Introduction

Surface sweet water has not increased for the past 20 years, and simultaneously, groundwater sources have been dropping [1]. Most of the natural resources of drinking water are found to be contaminated with diverse toxic compounds and pathogenic microorganisms [2]. Approximately 1 billion people across the planet face water scarcity, and it is estimated that this problem will touch approximately 2 billion people by 2025 [3]. According to the World Health Organization (WHO) report, water borne diseases kill nearly 12 million people every year [4]. A "carbon-free water" through artificial methods has therefore become a necessity for the survival of the human race.

The future of efficient water purification lies in Advanced Oxidation Processes (AOPs) in which pollutants are completely oxidized to CO_2, H_2O and mineral acids. According to many researchers, heterogeneous photocatalytic oxidation (PCO) is one of the most innovative, "green" and promising alternative technologies among oxidation processes [5–10]. There are several advantages that make it more attractive than other oxidative methods: (1) ambient temperature and pressure, (2) inexpensive and "easy to make" catalytic materials, (3) mild oxidation conditions, (4) oxidative potential toward various contaminants [11]. Invariably, a good photocatalyst is described as photoactive, able to utilize visible and/or near UV light, biologically and chemically inert, photostable, inexpensive and non-toxic [12]. Among the group of metal oxides with these characteristics ZnO is growing in interest as a potential photocatalyst to compete with TiO_2. ZnO is one of many naturally oxygen deficient metal oxides that will photocatalytically decomposes complex organic molecules in the presence of UV illumination [13–15]. Recently, researchers have defined methods to create crystalline ZnO nanowires [16,17], nanorods [18,19], nanotubes [20], nanobelts [21,22], nanotowers [23], dendritic hierarchical structures [24] and an assortment of other structures [25]. However, only few of these studies addressed issues in deep photocatalysis investigations.

Grafting metal oxides (e.g., ZnO) nanoparticles onto different supports can change the properties of nanostructured metal oxide. In particular, type and textural characteristics of the material employed (the support) may affect important physical and chemical properties of the final photocatalytic system that act as rate determining steps: absorption of light, adsorption–desorption equilibria of reaction intermediates, and control of the diffusion of reactants and products in or out of catalytic sites located inside of a porous network. It is in this context that recent developments in the discovery of new supports (in combination with novel synthetic procedures) for the preparation of hybrid materials with well-defined structures at the nanometer scale may afford better

* Corresponding author. Tel.: +48 22 343 3215.
E-mail address: jcarloscolmenares@ichf.edu.pl (J.C. Colmenares).

http://dx.doi.org/10.1016/j.apcatb.2015.01.031
0926-3373/

design of active sites for catalytic processes, including photocatalytic processes [26]. Of course, another main role of a solid support is that the photocatalysts become more easily handled and recycled. In this context, the coupling of photocatalysis with filter separation has emerged as a promising water treatment process [27].

It is highly desirable to develop simple, low-cost and low-temperature processes for controllable synthesis of photocatalytic active ZnO nanostructures on alternative substrates [28,29]. Self-cleaning polymeric fibers have been successfully prepared by depositing ZnO nanoparticle onto wool and polyacrylonitrile (PAN) fibers with good compatibility and significant photocatalytic self-cleaning activity using the sol-gel process at ambient temperature [30].

This study focuses on the synthesis of one-dimensional (1D) ZnO nanorods onto a polypropylene (PP) nonwoven fiber mat. This prepared hierarchical fiber/nanorod crystal composition with surface-normal ZnO nanorods on the cylindrical fiber template was tested in the photocatalytic mineralization of phenol in water. The hierarchical structure shows superior photocatalytic performance than the commercial ZnO counterpart. This study should be beneficial to the development of processes that involve the use of polymeric fibers in a photocatalytic environment.

2. Experimental

2.1. Photocatalysts' synthesis

The compound used as model water contaminant was phenol (99%) purchased from Alfa Aesar. Zinc oxide (99%) and zinc acetate (dihydrate) were supplied by Chempur (Poland). All other reagents, of chemical grade, were purchased from Avantor Performance Materials (Poland) and used without any further purification.

Hydrothermal method utilized in this paper is widely used to obtain different morphological structures of zinc oxide at different surfaces [31–33]. In this study ZnO (6 wt.%) was deposited on the network of nonwoven material. Commercially available nonwoven filtering material obtained using melt-blown technique from polypropylene (PP) homopolymer (Borealis Borow HL504FB) was used in our investigations. The material was modified with zinc oxide using a three-step method: (a) plasma treatment, (b) modification of PP fabrics by thin layer ZnO nuclei, and (c) growing of ZnO nanorods on the modified surface. Initial material has been treated by plasma discharge to improve wettability and adhesion of nano-nuclei to polymer surface [34,35]. This process was conducted in DIONEX Series 2000 reactor with radio frequency plasma generator in vacuum and oxygen. In order to select process parameters, which allow to improve wettability of PP fabrics (contact angle deg. obtained 135 ± 6) without polymer fibers degradation, different power and time settings were used: (a) 50 W discharge by 3 min (contact angle deg. obtained 110 ± 6), (b) 25 W by 5 min (contact angle deg. obtained 107 ± 8) and (c) 50 W by 5 min (contact angle deg. obtained 105 ± 6). The influence of plasma treatment on contact angle between water and the materials' surface (obtained results in parenthesis) was investigated by goniometer observations of water droplets. For each sample at least 10 droplets were placed on nonwovens surface.

Zinc oxide nuclei were synthesized by reacting zinc acetate and sodium hydroxide in isopropanol medium. The reaction was carried out at a temperature of 60 °C under continuous stirring for 2 h. Nanoparticles dispersion was used to modify polypropylene fibers by immersion method. The modified nonwovens were dried at 50 °C and annealed at 145 °C during 3 s. ZnO nanorods are grown on fibers surface by wet chemical decomposition of complex consisting of hexa(methylenetetramine) and zinc nitrate in aqueous solution. The reaction mixture was heated up to 90 °C for 5 h and then the samples were washed in distilled water and dried at 30 °C.

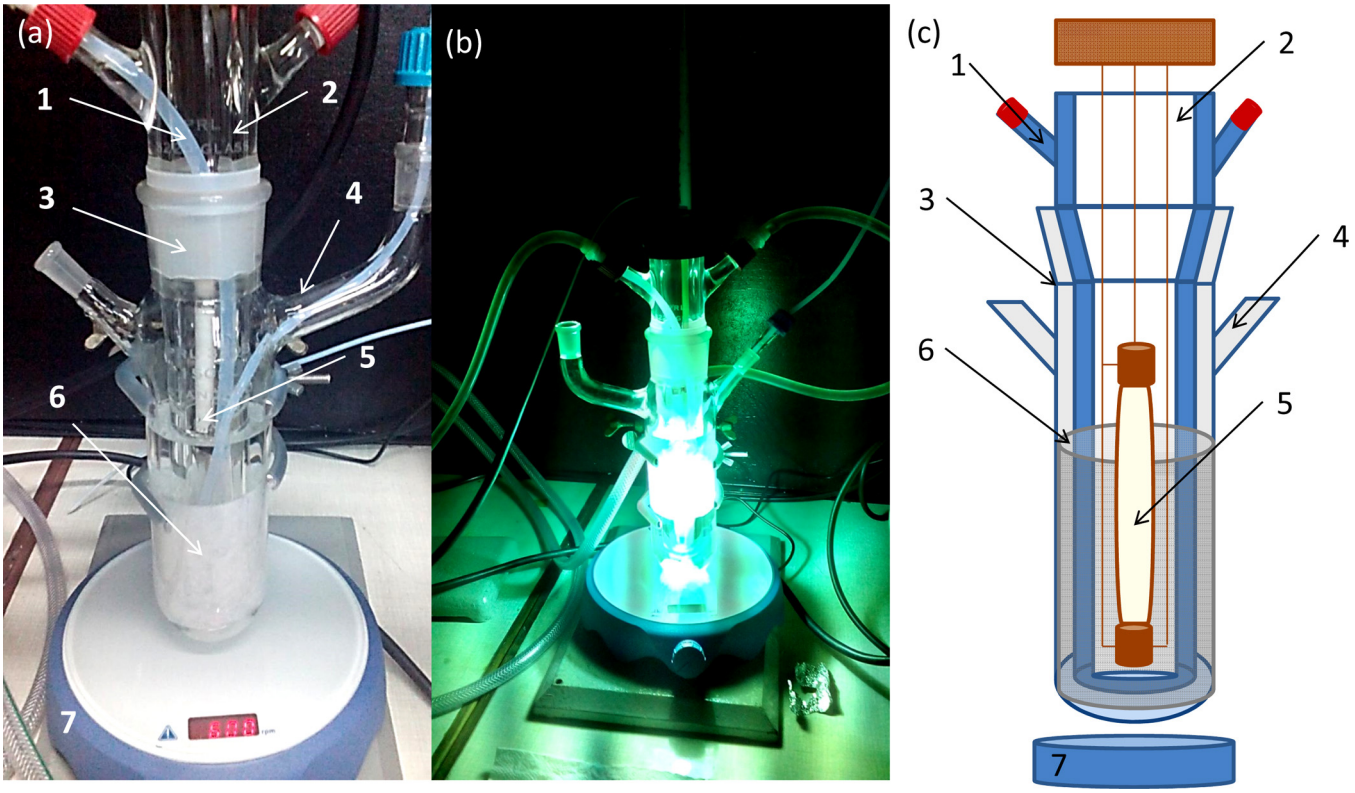

Fig. 1. Photocatalytic reaction system before (a) during (b) the reaction, and schematic representation of the photocatalytic reaction system (c); (1) lamp cooling system (2) double-walled immersion well (3) photoreactor (4) port for taking samples (5) 125 W UV lamp (6) photocatalyst (7) magnetic stirrer.

Table 1
Summary of the textural and optical features of the photocatalysts.

Materials	BET/BJH			UV–vis	
	S_{BET} [$m^2\ g^{-1}$]	BJH V_p [$mL\ g^{-1}$]	BJH dp [nm]	Band gap [eV]	Absorption threshold [nm]
p-PP	0.2643	0.000372	64.13	–	–
PP	0.3681	0.000571	27.47	–	–
ZnO/PP	0.7958	0.004005	44.39	3.17	390
Commercial ZnO	18.8371	0.072792	175.305	3.18	389

S_{BET} – specific surface area, V_p – the adsorbed volume, dp – pore diameter.

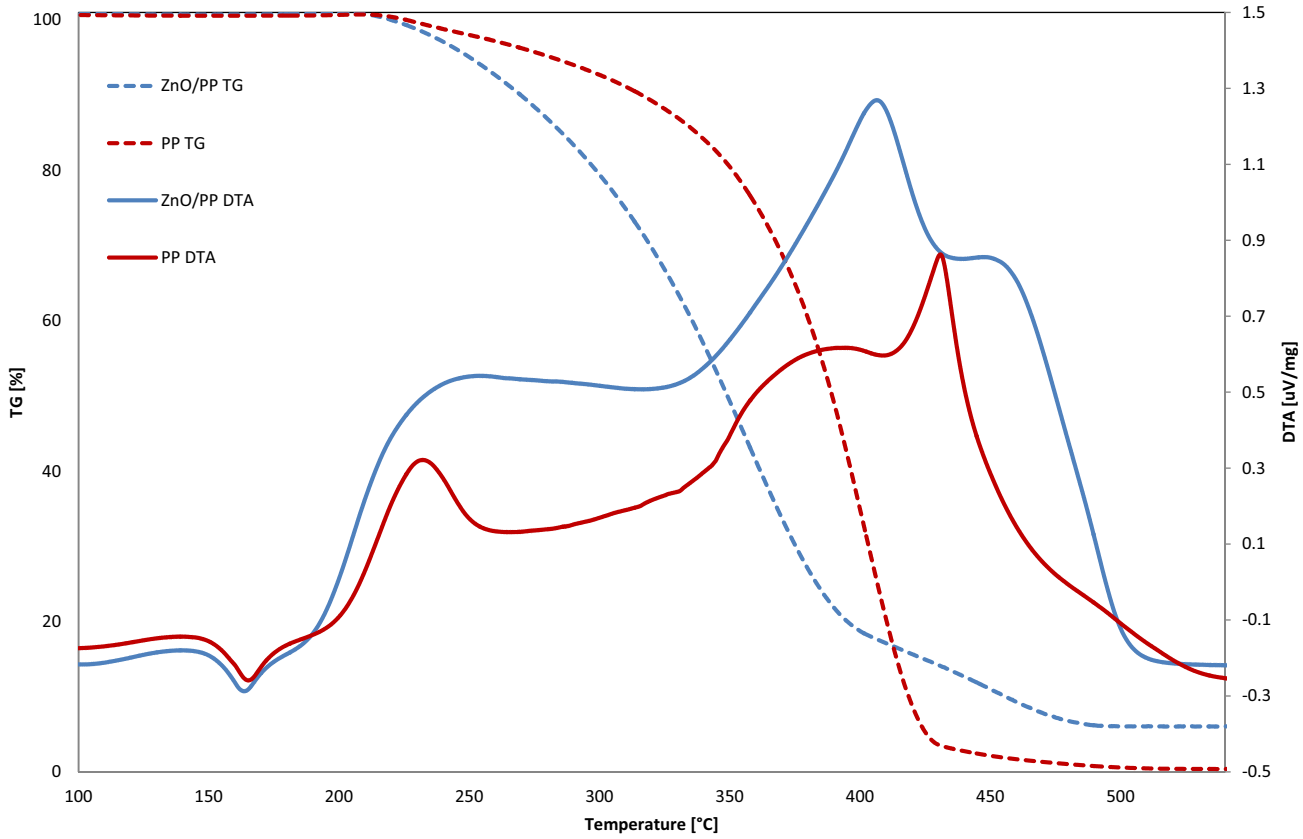

Fig. 2. TGA thermogram of ZnO/PP and PP fabrics.

2.2. Photocatalytic test

The photoactivity of polypropylene reference material (PP), polypropylene modified with zinc oxide (ZnO/PP) and commercial ZnO was studied by the degradation of phenol aqueous solution. All reactions in aqueous phase were conducted in a standard photochemical reaction flask (Model PRL 3303, Fig. 1) with a total solution volume of 150 mL. A lamp of medium pressure 125 W (Model RQ 3010, Photochemical Reactors Ltd., UK, λ_{max} = 365 nm), located in a vertical position and supplied with double-walled vessels made of borosilicate glass (Model PRL 3220 Glass), was used for illumination (Fig. 1). The batch photoreactor system was stirred magnetically at 600 rpm and the reaction temperature was established at 30 °C. The phenol solutions (50 ppm) were prepared using Milli-Q water. Photocatalytic filter materials were cut into rectangular pieces (15 cm × 7 cm, total area 105 cm^2) and placed around the walls inside the reactor (Fig. 1(a)). The experiments were carried out under ambient air (no oxygen bubbling conditions). In order to equilibrate the adsorption–desorption of phenol over the photocatalyst surface, the reaction solution was left in the dark for

Table 2
Photocatalysts activities in aqueous phase phenol degradation (conditions: 150 mL of mother solution, C_{phenol} = 50 ppm, T = 30 °C, reaction pressure 1 bar, 125 W UV lamp, irradiation time: 4 h).

	Photolysis	ZnO	PP	ZnO/PP 1st cycle	ZnO/PP 2nd cycle	ZnO/PP 3rd cycle
Phenol conversion [%]	22	53	39	54	74	76
Initial specific reaction rate[a] [$ppm/s\ m^2$]	–	0.69	0.79	2.12	–	–

[a] For the first 20 min of reaction.

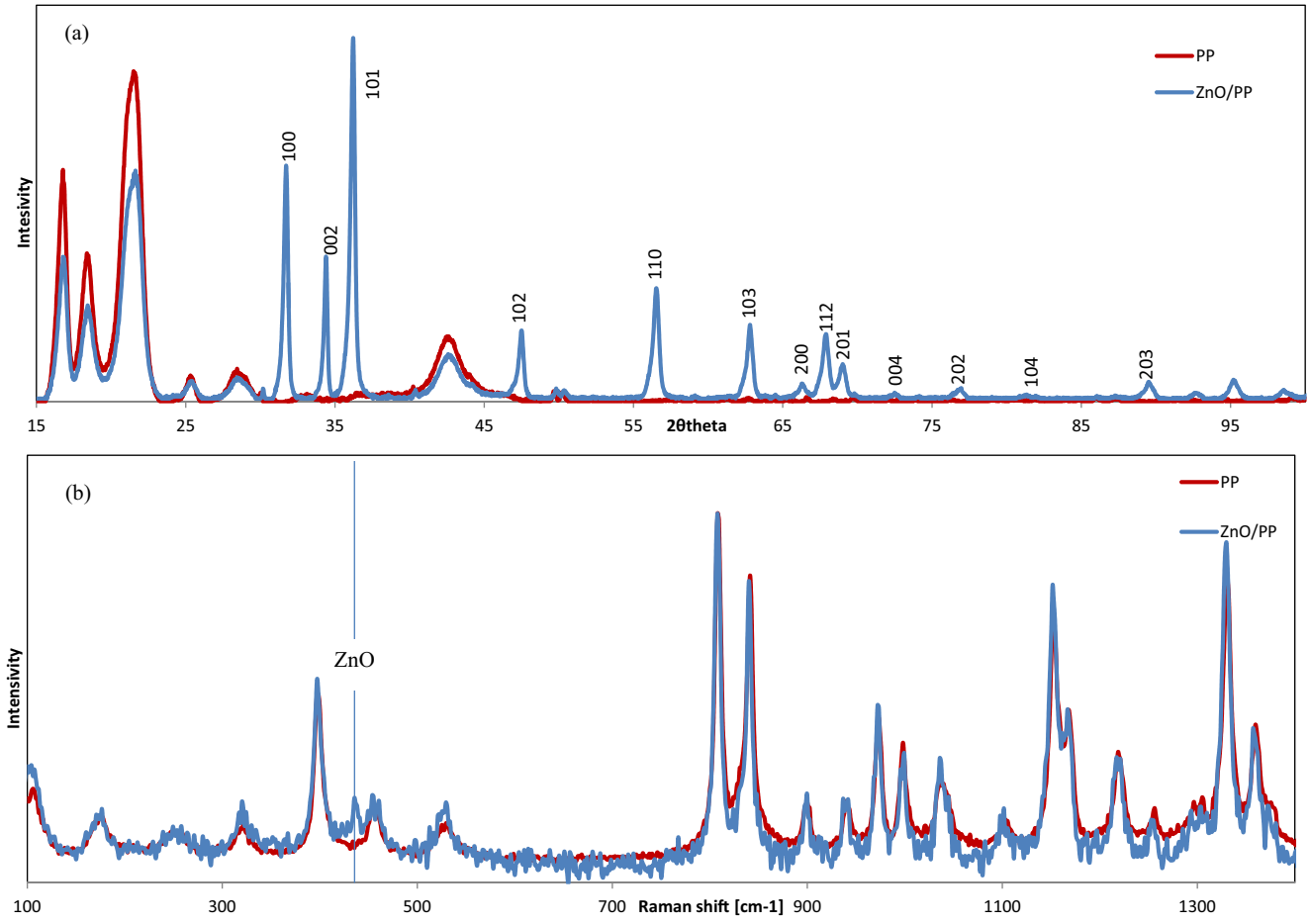

Fig. 3. (a) X-ray diffraction pattern and (b) Raman spectra of ZnO/PP and PP fabrics.

20 min before each reaction. All photocatalytic reactions and control experiments were repeated three times in order to estimate standard deviation.

Approximately samples of 1 mL were collected directly from the photoreactor at specific time intervals and filtered (0.20 μm, 25 mm, nylon filters). The concentration of phenol was determined by a high performance liquid chromatography (HPLC, Waters Model 590 pump) equipped with a Dual Absorbance Detector (Waters 2487) and a XBridge™ C18 (5 μm, 150 mm length, 4.6 mm inner diameter) column provided by Waters. The injection volume was 10 μL. The mobile phase was Milli-Q water/methanol in the ratio of 65:35 (v/v) with 0.1% of CF_3COOH, used in isocratic elution at a flow rate of 1 mL/min.

It was applied a ICP MS (Elan 6100 DRC SciexPerkinElmer spectrometer) technique with ionic plasma detection in order to determine the amount of zinc ions present in aqueous solution after 4 h of radiation. Chemical oxygen demand was performed to study the photostability of the nonwovens under UV-light. The tests were conducted using COD photometer AL250, with measuring range from 0 to 150 mg/L O_2. The results showed the amount of oxygen consumed in total chemical oxidation of the organic component in the aqueous solution, after 30, 120 and 240 min reaction in the presence of ZnO/PP and polypropylene fiber after plasma treatment (p-PP) (Table 3).

2.3. Characterization of photocatalysts

The specific surface areas, pore volumes and average pore diameters were determined by N_2 physisorption using a Micromeritics ASAP 2020 automated system and the Brunauer–Emmet–Teller (BET) and the Barret–Joyner–Halenda (BJH) methods. Samples were double degassed under vacuum (0.1 Pa) for 5 h at 100 °C prior to adsorption measurements.

X- ray diffraction was used to check phase composition of photocatalysts. Analysis was carried out with a Bruker D8 Advance X-ray diffractometre using Ni- filtered CuKα radiation (λ = 1.541874 Å) at

Table 3
Stability studies of the photocatalytic support (PP = polypropylene) by chemical oxygen demand tests.

Illumination time [min]	Total COD for ZnO/PP [mg/L]	Estimate COD for phenol[a] [mg/L]	Total COD [mg/L]	Intermediates [mg/L]	COD for carbon dioxide[b] [mg/L]	Total COD for p-PP [mg/L]
0	0	119	119	±0	29	0
30	10	103	116	±3		<Lo[c]
120	11	85	106	±11		3
240	15	70	90	±5		<Lo[c]

[a] Calculated from HPLC results.
[b] After 4 h reaction.
[c] Lo – result below the lowest limit of the measuring range.

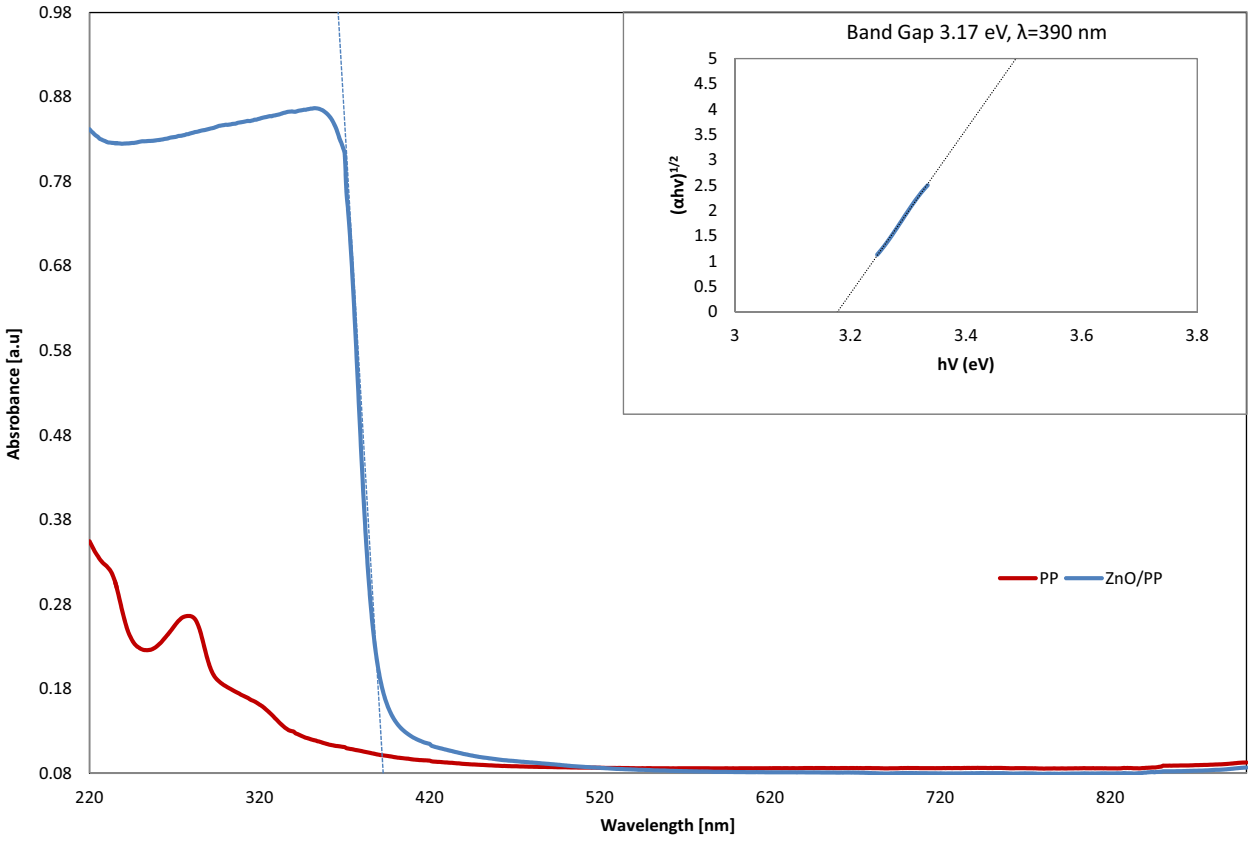

Fig. 4. Diffuse reflectance UV-visible spectra of PP, ZnO/PP and plot of transformed Kubelka–Munk function versus the energy of the light absorbed for ZnO/PP (inset).

40 kV and 40 mA. The diffraction angle 2θ in the range of 15°–100° was scanned at a rate of 0.025° per second. The most intense peak of XRD spectrum was used to calculate the average crystallite size according to the Scherrer equation (Eq. (1)),

$$D = \frac{K\lambda}{\beta\cos\theta} \quad (1)$$

where D is the average crystallite size of the catalyst (nm), λ is the wavelength of the CuKα X-ray radiation ($\lambda = 0.15406$ nm), K is a Scherrer constant customarily set as 0.94, β is the full width at a half maximum (FWHM) intensity of the peak observed at 2θ (radian), and θ is the diffraction angle. The presence of zinc oxide in modified polypropylene material was also confirmed by Raman Spectroscopy.

The Raman Spectra were performed on Renishaw inVia Raman Microscope which is supplied with 50× long working distance objective. Raman date were recorded at room temperature with the 10% laser power excitation source ($\lambda = 514$ nm) over range 100–3200 cm^{-1} and exposure time of 10 s.

UV–vis diffuse reflectance spectra were recorded on UV/VIS/NIR spectrophotometer Jasco V-570 equipped with an integrating sphere. The baseline was recorded using Spectralon™ (poly(tetrafluoroethylene) as a reference material). To determine the band gap function, the Kubelka–Munk method based on the diffuse reflectance spectra was employed. The E_g was calculated form $(f(R)h\nu)^{1/2}$ versus $h\nu$ plots. The function $f(R)$ was calculated from the equation (Eq. (2)),

$$f(R) = \frac{(1-R)^2}{2R} \quad (2)$$

Thermogravimetric analyzer (NETZSCH STA 449 C Jupiter) was used in TGA/DTA mode to determine thermal stability and the percentage composition of modified materials. The measurement was done under air flow rate of 60 mL/min at a heating rate of 5 °C/min. The scanning temperature was acquired in the range from 35 to 600 °C.

High resolution scanning electron microscope (HR-SEM) Hitachi SU8000 was used to determine the morphology of the samples.

3. Results and discussion

3.1. Physico-chemical properties of the photocatalysts

As shown in the Section 2, in the case of all plasma treated samples, contact angle in water is lower than that for reference sample, what indicates a positive influence of plasma treatment for increasing surface energy. For further processing we have chosen 50 W by 5 min (contact angle deg. obtained 105 ± 6 which resulted in 30° decreased in comparison to untreated PP) as the best parameters used to prepare p-PP nonwovens.

The seed layer in nonwoven PP filters presents nucleation sites (results not shown), lowering the thermodynamic barrier for ZnO nano- and micro-crystal growth and further enhancing the growth direction selectivity and aspect ratio [23,36].

TGA thermogram of PP and ZnO/PP in air atmosphere is shown in Fig. 2. The melting point temperature for both samples is about 164–165 °C and is consistent with theoretical value. A mass difference through the thermal decomposition between of ZnO/PP and reference PP is approximately 6 wt.% of ZnO with 94 wt.% of polypropylene. In Fig. 2. it is observed an exothermic effect at 220–225 °C related to PP thermo-oxidative degradation but still does not involve mass loss as was ascribed by Golebiewski et al. [37], that it is typical behavior of thermo oxidative degradation of polypropylene. The peak observed at approximately 400 °C (Fig. 2)

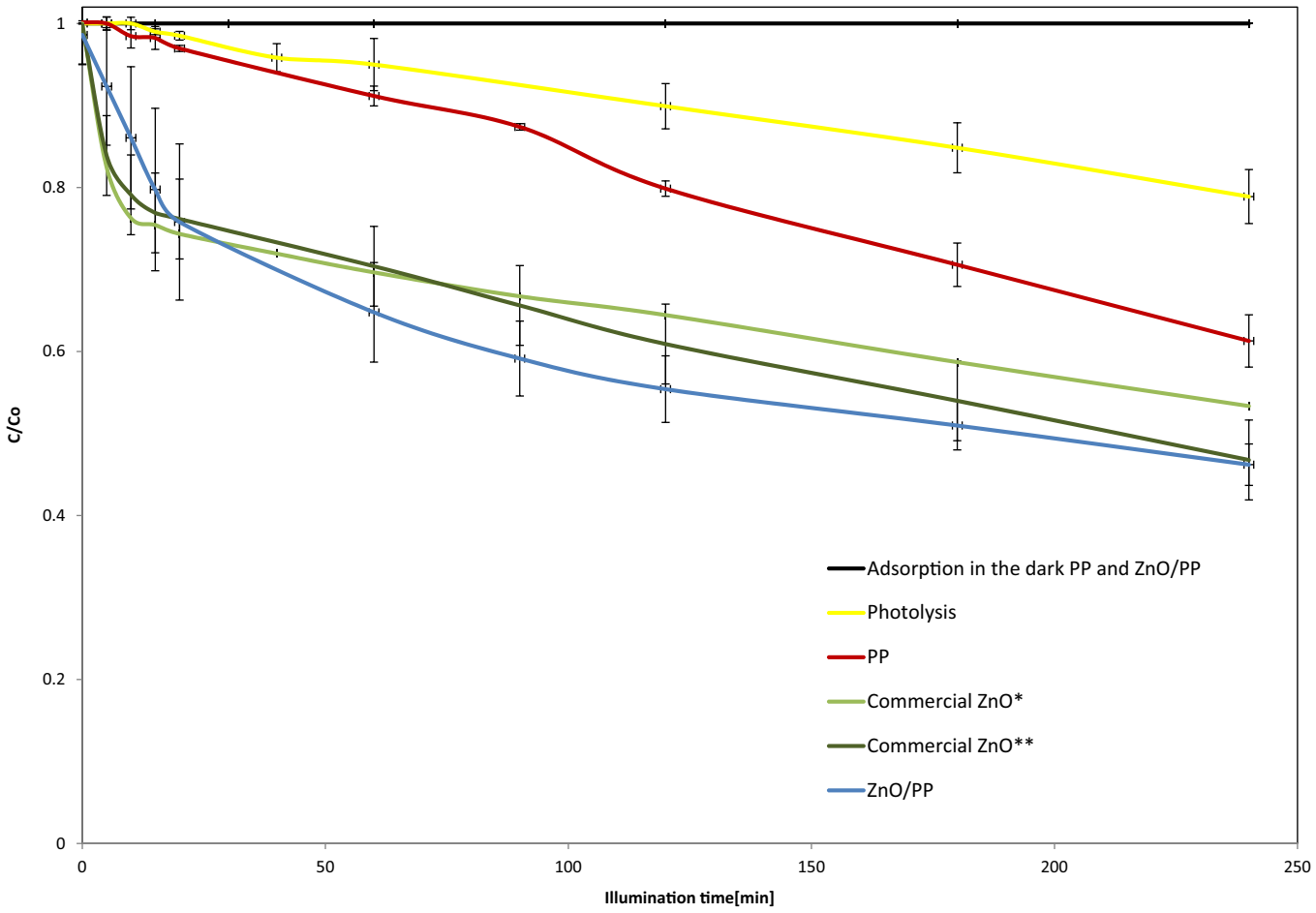

Fig. 5. Degradation profiles of phenol in water (*64 mg amount of zinc oxide equal 6 wt.% of hybrid ZnO/PP, **loading: 1 g/L).

is concerned to the total decomposition/oxidation of polypropylene support [38].

The nitrogen adsorption–desorption isotherms (not shown) were carried out for PP and ZnO/PP samples and are of type IV with H3 hysteresis loops which is associated with mesoporous structure (according to the IUPAC classification). The pore size distribution of p-PP indicates on type II isotherm, which is the typical shape attributed to adsorption into macroporous [39,40]. The average pore diameter size, pore volume and the specific surface area values are reported in Table 1 and it is seen a surface area of ZnO/PP larger than reference PP which is favorable in photocatalysis reaction and can impact its efficiency. Polypropylene fabric p-PP exhibited the opposite behavior, textural parameters were reduced after plasma treatment.

Crystalline phase composition of the reference nonwoven polypropylene filter after modification with zinc oxide is shown in Fig. 3a. The X-ray patterns of ZnO/PP present the typical α-form PP crystals and the main reflections at 2θ values of 31.8, 34.4, 36.3, 47.5, 56.6, 62.9, 68.0° can be respectively graded to (1 0 0), (0 0 2), (1 0 1), (1 0 2), (1 1 0), (1 0 3), and (1 1 2) crystal planes, which can be readily indexed to the pure hexagonal ZnO phase (JCPDS No. 36-1451) [41]. Crystallite sizes were calculated by Scherrer's equation and were 27 nm and 12 nm for ZnO and PP, respectively. The XRD results were compared and corroborate using Raman spectroscopy (Fig. 3b). It is reported that the hexagonal wurtzite structure of ZnO belongs to the space group C_{6v}^2, which predicts eight optical modes. In Fig. 3b it is observed Raman shift peak at 437 cm^{-1}, which is ascribed to the remarkable E_2(high) phonon mode of zinc oxide [42,43].

Diffuse reflectance UV–vis spectroscopy was used in order to determine the optical properties of tested materials. A characteristic absorption peak of ZnO/PP sample typically ascribed to zinc oxide is observed (Fig. 4). The band gap value is approximately 3.17 eV (Fig. 4, inset) and is in good agreement with literature [44]. Reference PP sample, in comparison with the ZnO/PP, exhibited a minimum absorption below 300 nm which didn't affect during our photocatalysis experiments (the used immersion well is made of borosilicate glass which acts as a filter for wavelength ≤300 nm).

3.2. Photocatalytic activity and stability

The results of phenol photodegradation reaction were compared with photolysis of phenol. The control experiments, carried out without nonwoven PP materials, were performed to confirm that the reaction efficiency depends on the presence of both light and photocatalyst. After 4 h of photolysis (without catalyst) the conversion was approximately 22%. Unmodified nonwoven PP and ZnO/PP were used in a dark adsorption test. After 4 h, in the absence of the light, the adsorption of phenol on surface was negligible (Fig. 5). Moreover, when the PP surface is illuminated it was observed a 39% phenol disappearance after 4 h (Fig. 5.) and this could be connected with the increase of PP wettability and surface free energy under UV light [45].

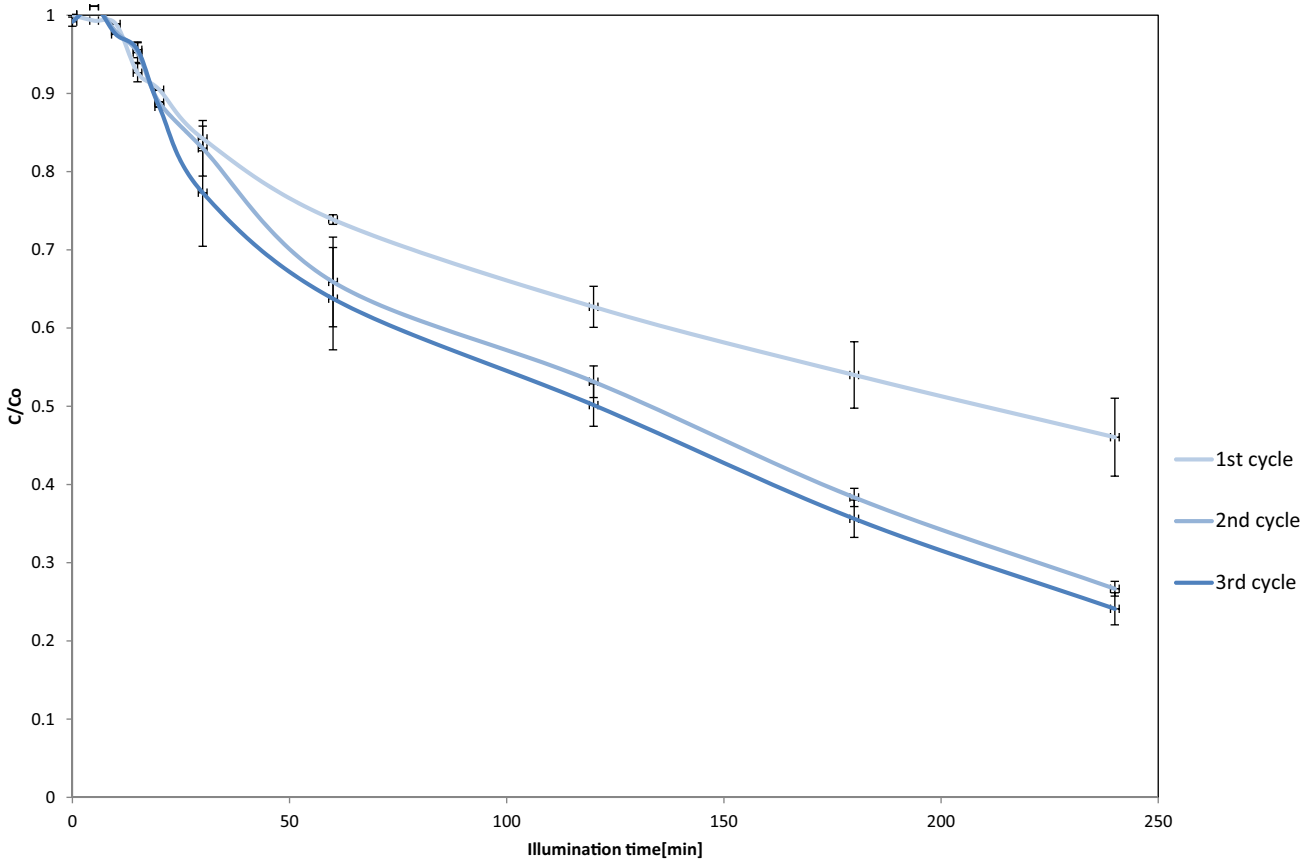

Fig. 6. Photocatalytic activity of ZnO/PP in aqueous phase phenol degradation with three times cycling uses (conditions: 150 mL of mother solution, C_{phenol} = 50 ppm, T = 30 °C, reaction pressure 1 bar, 125 W UV lamp, irradiation time: 4 h).

The photocatalytic performances of 1D ZnO nanorod on PP were very competitive in comparison with the commercial ZnO (after 4 h of illumination 54% and 53%, respectively). If we want to go through a more specific comparison between ZnO/PP and commercial ZnO, it can be seen that our hybrid material is more active than commercial ZnO due to the following reasons: (a) as we can see in the Fig. 5, the same mass of commercial ZnO used in the reaction (calculated based on the amount of ZnO in 6 wt.% ZnO/PP used in the test reaction) is much less active than the hybrid ZnO/PP material (after 4 h of illumination 47% and 54%, respectively), and (b) the initial specific rates (Table 2) calculated for ZnO and ZnO/PP are 0.69 and 2.12, respectively, what suggest that the hybrid material possess very high turn number (3.1-fold higher than ZnO) in photocatalytic activity for phenol degradation. Greatly enhanced ZnO/PP activity could be attributed to the following points:

- Well-defined vertical arrays structure of 1D ZnO nanorods possesses the characteristic of more active sites and light harvesting,
- The vertical 1D structure is benefit to shorten the electron transfer distance, thereby reducing the recombination probability of photo-induced electron–hole pairs, and
- The band bending between the interface of ZnO nanorods and PP can drive the photo-electrons flow to PP mat and also inhibit the recombination of electrons and holes.

Recyclability without loss of efficiency is an important parameter which is always considered for successful and economical large scale commercial application of the prepared photocatalyst. Therefore, simple and low-cost based techniques to maintain the efficiency of polymer-supported ZnO photocatalysts after several successive reuses is an issue of high importance. ZnO photocatalyst is well-known because the photocorrosion induced by the photogenerated holes, which leads to the poor photostability or deactivation during the long-term recycling use [46–48]. In an attempt to study the stability of our photocatalytic active hybrid ZnO/PP material, we carried out the following experiments:

i Three-times recycling test: for this purpose, after each cycle the photocatalyst was dried at 80 °C for 8 h and used in the next reaction. As it is seen in Fig. 6, ZnO/PP after the first cycle behaves very similar in terms of activity as commercial ZnO but interestingly is the fact that the activity of ZnO/PP (photodegradation of phenol) increases after the second (74% after 4 h of illumination) and third cycle (76%) in comparison with 53% for commercial ZnO. We believe that the improvement of the activity after the first cycle is due to the increase of ZnO/PP wettability and adsorptive properties. In other words, ZnO/PP photocatalytic oxidation active sites are more accessible within the whole ZnO/PP filter network for phenol to be degraded in water [49].

ii Polypropylene support stability: Chemical Oxygen Demand (COD) analysis and HR-SEM images were used to study the PP stability in ZnO/PP (Table 3, Fig. 7). The measurements indicate that trace amounts of the reference nonwoven material degrades during the reaction. This photo-oxidation of polypropylene is negligible and oscillates in approximately 0.43 wt.% after 1st cycle reaction. The estimated data based on COD analysis were consistent with weight loss of nonwovens after each reaction under UV irradiation. With the incorporation of ZnO nanoparticles into the PP matrix, the extent of photodegradation was significantly reduced. This is due to the superior UV light screening effects offered by the ZnO nanoparticles [50]. It was also observed that PP surface cracks were induced by photo-

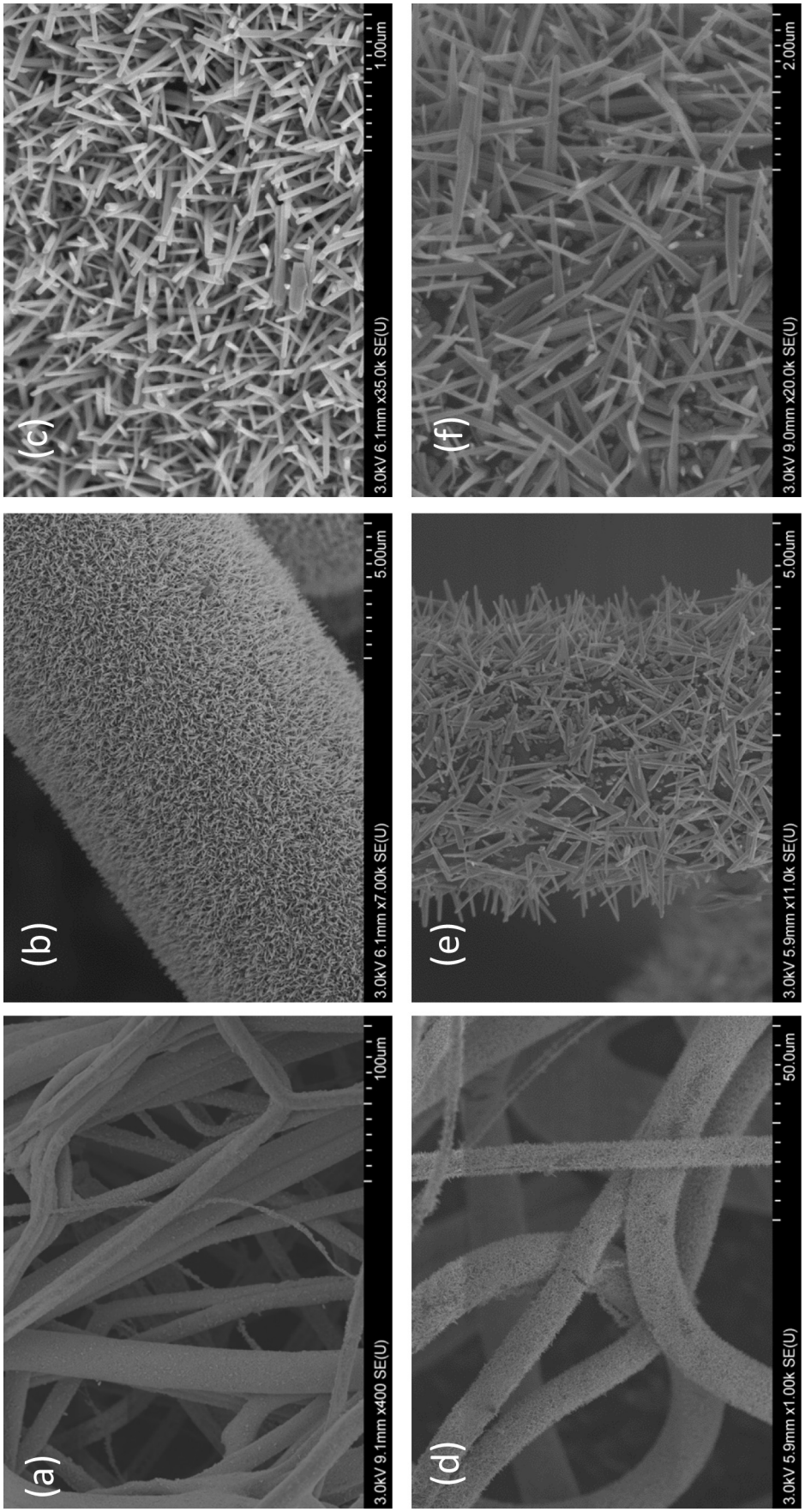

Fig. 7. HRSEM images of ZnO/PP before (a,b,c) and after (d,e,f) 3rd cycle reaction (conditions: 150 mL of mother solution, C_{phenol} = 50 ppm, T = 30 °C, reaction pressure 1 bar, 125 W UV lamp, irradiation time: 4 h).

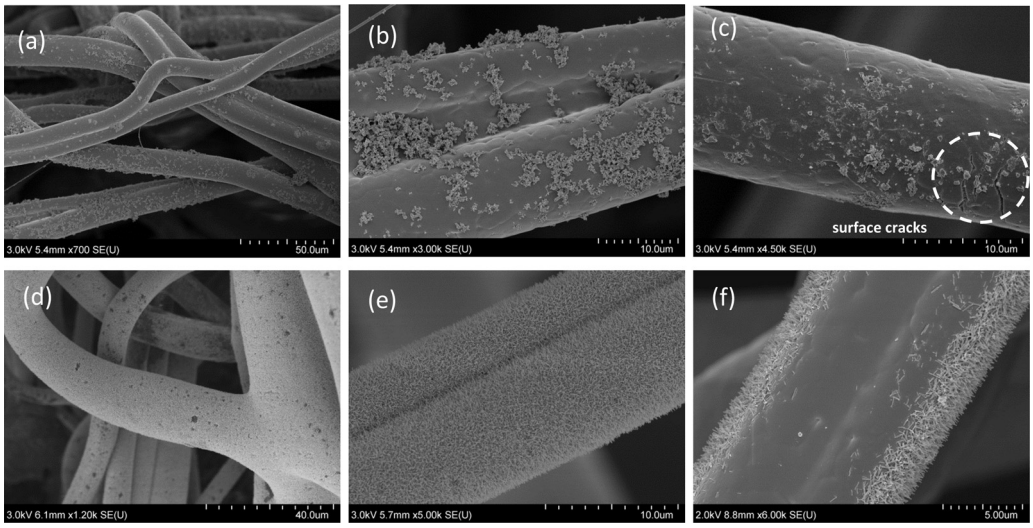

Fig. 8. HRSEM photocatalysts images before test reaction: (a,b) i-ZnO/PP, (d,e) ZnO/PP and after 3rd cycle test reaction: (c) i-ZnO/PP, (f) ZnO/PP; where (i-ZnO/PP) are fibers containing 6 wt.% zinc oxide obtained by wet impregnation method.

degradation when commercial ZnO was supported onto the p-PP surface by wet impregnation method (Fig. 8c). HR-SEM surface profile images (Fig. 8f) indicate that surface cracks were not observed in the case of 1D ZnO/PP nanocomposites after photocatalysis. Results from this research study indicate that the incorporation of ZnO nanoparticles into PP matrix can impart significant improvements on the photo-degradation resistance of PP to UV-irradiation. This remarkable information is not only important in the synthesis of very stable photocatalysts but also can have potential applications in others areas, for instance in new resistant and light materials for the building industry.

iii Zinc oxide stability: ICP-MS analysis was used for this study. As it is seen in Table 4 the amount of dissolved ZnO into water after three phenol degradation photocatalytic reactions (in total 46.50 mg (0.57 mmol) of ZnO after 12 h of three repeated reactions) is 8.62% of the ZnO initial amount in 1D ZnO/PP. For comparative purposes we checked also the leaching of ZnO in the case of ZnO/PP prepared by wet impregnation and we observed more than 3-fold (27.88%) ZnO leaching for this photocatalyst after three repeated cycles. We can firmly state that the 1D ZnO nanorods are more stable structures (please see HR-SEM images after reaction, Figs. 7 and 8) than the photocatalyst prepared using a conventional wet impregnation method. This finding additionally indicates that the method of photocatalyst synthesis is also very important.

Table 4
ICP-MS analysis of the percentage of Zn leached to aqueous phase during 4 h illumination (125 W, $\lambda = 365$ nm).

	Amount of zinc in solution [ppm]	Percentage of leached Zn [%]
Millipore Water[a]	2.94×10^{-3}	–
ZnO/PP 1st cycle[b]	11.20	2.54
ZnO/PP 2nd cycle[b]	12.18	2.90
ZnO/PP 3rd cycle[b]	13.97	3.18
	37.35	8.62

[a] Zinc content in pure water.
[b] Data measured for ZnO/PP in phenol solution (50 ppm).

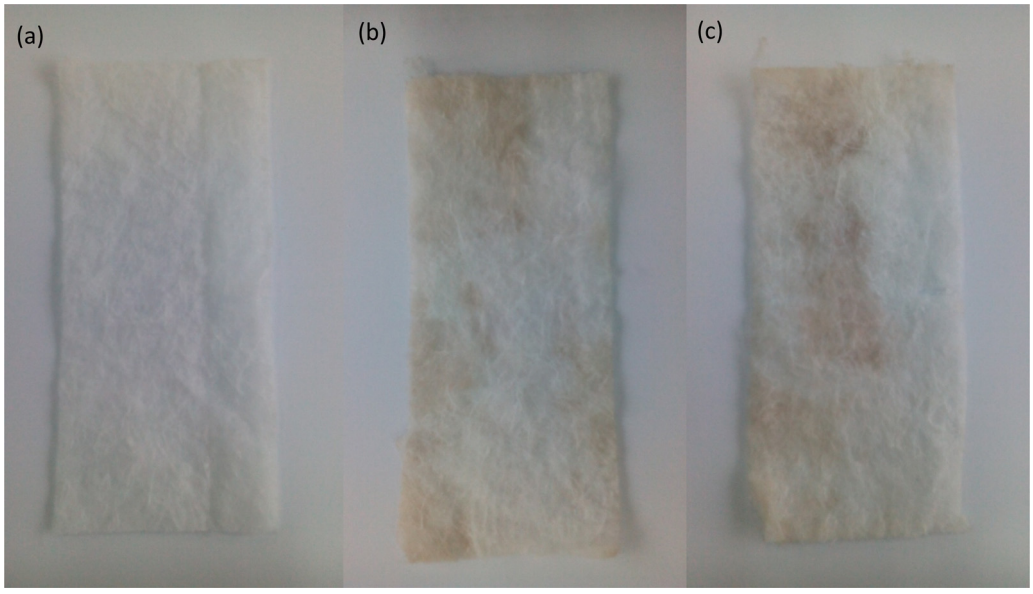

Fig. 9. Photocatalytic mats used: (a) ZnO/PP before reaction, (b) after 1st cycle (dried for 8 h at 80 °C), and (c) after 2nd cycle (dried for 8 h at 80 °C).

In Fig. 9 pictures of the ZnO/PP are presented before and after reaction. It is clearly seen that after reaction there are a kind of "brown spots" which can be attributed to the partial superficial oxidation (or epoxidation) of PP in places where ZnO leaching is more pronounced. Superoxide radical and hydroxyl radical are formed during photocatalysis reaction and they can oxidize some propylene monomer units and lead to create double bonds between adjacent carbons [37]. This causes a change of color of the surface of ZnO/PP material in the form of "brown spots" (Fig. 9). However, the percentage of PP photodegradation is negligible and occurs only on the surface layer of nonwoven as it was proved by COD test.

4. Conclusions

It has been proved the effective photocatalytic activity in aqueous phase phenol degradation of 1D ZnO/PP hybrid material synthesized by a simple physico-chemical methodology.

Radio frequency plasma treatment in oxygen atmosphere allows for improvement of polypropylene liquid contact angle. Such modification is essential for coating PP fibers with ZnO nanorods in uniform manner and with high activity and stability in aqueous phase photocatalytic degradation of phenol.

This research is an important step forward in the preparation of photocatalytic active filters (the combination of the advantages from photocatalysis and filtration) for water purification.

Acknowledgement

Project supported by a grant from Switzerland through the Swiss Contribution to the enlarged European Union.

References

[1] (DOE), U.D.E.U. Energy Demands on Water Resources: Report to Congress on the Interdependency of Energy and Water. US DOE, Washington, DC, 2006.
[2] S. Baruah, J. Dutta, Environ. Chem. Lett. 7 (3) (2009) 1–14.
[3] (UN), U.N. International Decade for Action Water for Life, 2005–2015: Water Scarcity, 2010.
[4] http://www.who.int/infectious-diseasereport/pages/textonly.html (accessed 26.07.12).
[5] L. Zou, Y. Luo, M. Hooper, E. Hu, Chem. Eng. Prog. 45 (2006) 959–964.
[6] G.M. Zuo, Z.X. Cheng, H. Chen, G.W. Li, T. Miao, J. Hazard. Mater. B 128 (2006) 158–163.
[7] W.K. Jo, J.H. Park, H.D. Chun, J. Photochem. Photobiol. A Chem. 148 (2002) 109–119.
[8] F. Benoit-Marquie, U. Wilkenhoner, V. Simon, A.M. Braun, E. Oliveros, M.T. Maurette, J. Photochem. Photobiol. A Chem. 132 (2000) 225–232.
[9] D.I. Kondarides, A. Patsoura, X.E. Verykios, J. Adv. Oxid. Technol. 13 (2010) 116–123.
[10] D.S. Bhatkhande, V.G. Pangarkar, A.A.C.M. Beenackers, J. Chem. Technol. Biotechnol. 77 (2001) 102–116.
[11] S.B. Sadale, K. Noda, K. Kobayashi, K. Matsushige, Appl. Surf. Sci. 257 (2011) 10300–10305.
[12] M. Hussain, N. Russoa, G. Saraccoa, Chem. Eng. J. 166 (2011) 138–149.
[13] N. Daneshvar, D. Salari, A.R. Khataee, J. Photochem. Photobiol. A 162 (2004) 317–322.
[14] B. Pal, M. Sharon, Mater. Chem. Phys. 76 (2002) 82–87.
[15] C.S. Turchi, D.F. Ollis, J. Catal. 122 (1990) 178–192.
[16] L.E. Greene, M. Law, J. Goldberger, F. Kim, J.C. Johnson, Y.F. Zhang, R.J. Saykally, P.D. Yang, Angew. Chem. Int. Ed. 42 (2003) 3031–3034.
[17] Y. Li, G.W. Meng, L.D. Zhang, F. Phillipp, Appl. Phys. Lett. 76 (2000) 2011–2013.
[18] J.J. Wu, S.C. Liu, Adv. Mater. 14 (2002) 215–218.
[19] B. Gong, Q. Peng, J.S. Na, G.N. Parsons, Appl. Catal. A 407 (2011) 211–216.
[20] L.F. Xu, Q. Liao, J.P. Zhang, X.C. Ai, D.S. Xu, J. Phys. Chem. C 111 (2007) 4549–4552.
[21] M.S. Arnold, P. Avouris, Z.W. Pan, Z.L. Wang, J. Phys. Chem. B 107 (2003) 659–663.
[22] Z.R. Dai, Z.W. Pan, Z.L. Wang, Adv. Funct. Mater. 13 (2003) 9–24.
[23] Y.H. Tong, Y.C. Liu, C.L. Shao, R.X. Mu, Appl. Phys. Lett. 88 (2006) 11–123.
[24] L. Vayssieres, K. Keis, S.E. Lindquist, A. Hagfeldt, J. Phys. Chem. B 105 (2001) 3350–3352.
[25] J.S. Na, B. Gong, G. Scarel, G.N. Parsons, ACS Nano 3 (2009) 3191–3199.
[26] F.J. Zaera, Phys. Chem. Lett. 1 (2010) 621–627.
[27] S. Singh, H. Mahalingam, P.K. Singh, Appl. Catal. A 462–463 (2013) 178–195.
[28] C. Han, Z. Chen, N. Zhang, J.C. Colmenares, Y.-J. Xu, Adv. Funct. Mater. 25 (2015) 221–229.
[29] M. Francavilla, A. Pineda, M. Franchi, A.A. Romero Reyes, M. Monteleone, J.C. Colmenares, C. Vargas, R. Luque, Green Chem. 16 (2014) 2876–2885.
[30] H.F. Moafi, A.F. Shojaie, M.A. Zanjanchi, J. Appl. Polym. Sci. 121 (2011) 3641–3650.
[31] Y.B. Kwon, S.W. Shin, H.-K. Lee, J.Y. Lee, J.-H. Moon, J.H. Kim, Curr. Appl. Phys. 11 (2011) 197–201.
[32] G. Kenanakis, D. Vernardou, N. Katsarakis, Appl. Catal. A. 411–412 (2012) 7–14.
[33] H.-S. Choi, M. Vaseem, S.G. Kim, Y.-H. Im, Y.-B. Hahn, J. Solid State Chem. 189 (2012) 25–31.
[34] R. Chen, Y. Bayon, J.A. Hunt, Colloid Surf. B 96 (2012) 62–68.
[35] Y. Li, W. Shi, S. Li, M. Lei, Surf. Coat. Technol. 213 (2012) 139–144.
[36] L. Vayssieres, K. Keis, S.-E. Lindquist, A. Hagfeldt, J. Phys. Chem. B 105 (2001) 3350–3352.
[37] J. Golebiewski, A. Galeski, Compos. Sci. Technol. 67 (2007) 3442–3447.
[38] C.L. Beyler, M.M. Hirschler, Thermal decomposition of polymers, in: SFPE (Ed.), The SFPE Handbook of Fire Protection Engineering, 3rd ed., National Fire Protection Association, Quincy, MA, 2002, pp. 1–131.
[39] A. Cireli, M. Mutlu, B. Kutlu, N. Onar, I. Kayatekin, E. Celik, Sol-gel coatings of plasma modified polypropylene fabric for gas defence, In: Proceedings of the 3rd European Conference on Protective Clothing and Nokobetef 8, Gdynia, Poland, 2006, CIOP-PIB.
[40] Z. Zhang, C. Shao, X. Li, L. Zhang, H. Xue, C. Wang, Y. Liu, J. Phys. Chem. C 114 (2010) 7920–7925.
[41] B. Weng, M.-Q. Yang, N. Zhang, Y.-J. Xu, J. Mater. Chem. A 2 (2014) 9380–9389.
[42] Y. Huang, M. Liu, Z. Li, Y. Zeng, S. Liu, Mater. Sci. Eng. B 97 (2003) 111–116.
[43] K. Pan, Y. Dong, W. Zhou, Q. Pan, Y. Xie, T. Xie, G. Tian, G. Wang, ACS Appl. Mater. Interfaces 5 (2013) 8314–8320.
[44] V. Srikant, D.R. Clarke, J. Appl. Phys. 83 (1998) 5447–5451.
[45] K. Gotoh, S. Kikuchi, Colloid. Polym. Sci. 283 (2005) 1356–1360.
[46] B. Weng, M.-Q. Yang, N. Zhang, Y.-J. Xu, J. Mater. Chem. A 2 (2014) 9380–9389.
[47] Z.B. Yu, Y.P. Xie, G. Liu, G.Q. Lu, X.L. Ma, H.-M. Cheng, J. Mater. Chem. A 1 (2013) 2773–2776.
[48] C. Han, M.-Q. Yang, B. Weng, Y.-J. Xu, Phys. Chem. Chem. Phys. 16 (2014) 16891–16903.
[49] R. Sun, A. Nakajima, A. Fujishima, T. Watanabe, K. Hashimoto, J. Phys. Chem. B. 105 (2001) 1984–1990.
[50] H. Zhao, R.K.Y. Li, Polymer 47 (2006) 3207–3217.